Simplified Thermal Model of PM Motors in Hybrid Vehicle Applications Taking into Account Eddy Current Loss in Magnets

Xiaofeng Ding [1], Madhur Bhattacharya [2], and Chris Mi [3]

[1] *Department of Electrical and Computer Engineering, University of Michigan-Dearborn, dxf_219@163.com*
[2] *Department of Electrical and Computer Engineering, University of Michigan-Dearborn, busundi@hotmail.com*
[3] *Department of Electrical and Computer Engineering, University of Michigan-Dearborn, mi@ieee.org*

Abstract

Permanent Magnet (PM) Motors are popular choices for hybrid electric vehicle (HEV) powertrain applications. The effects of the excessive heat in the magnets can degrade the performance of these machines if not dealt properly. It is therefore critical to develop a complete and representative model of the heat processes in the electric motors. In this paper, a simplified analytical model is developed as a thermal circuit with a network of interconnected nodes and thermal resistances representing the heat processes within the SPMSM. Both losses induced by sinusoidal and PWM waveform voltage supplies are calculated respectively as heat sources in the thermal circuit. Because temperature-rise inside the magnets caused by eddy current loss can lead to the unpredictable deterioration of the magnets, the circuit takes into consideration the eddy current loss developed in the permanent magnets. The thermal circuit is then solved in MATLAB through a system of linear equations. The results of the analytical model are confirmed through 3-D finite element analysis (FEA) simulation in Ansoft ePhysics software.

Keywords

hybrid electric vehicle, surface permanent magnet synchronous motors, thermal circuit, heat processes, pulse-width-modulated

1. INTRODUCTION

Permanent magnet (PM) motors are popular choices for hybrid electric vehicle (HEV) powertrain applications. Until recently, there has been a large emphasis on the electromagnetic properties of such a motor. However, due to the danger of demagnetization [Yoshida et al., 2000; Ishak et al., 2005] over the lifetime, the thermal impact on the magnets needs to be thoroughly understood. The optimal design of electrical motors with solid thermal characteristics will provide improved efficiency and power densities in traction vehicle. Such vehicles rely on high torque meaning increasing current and inevitable rise in temperatures in the motor. The thermal complexities involved in designing PM motors for HEV applications require a breakdown of the individual thermal components in the system.

Thermal studies on electric motors often approach the subject using FEA. Although the time stepped FEA provides greater accuracy by accumulating the thermal distribution over minor elements, it remains relatively time-consuming and does not provide as much insight as an analytical solution [Mellor and Turner, 1991; Taylor, 1935; Gazley, 1958; Boglietti et al., 2002; Sai et al., 2005; Sooriyakumar, et al., 2007; Staton et al., 2005; Guo et al., 2005; Funieru and Binder, 2008; Staton and Cavagnino, 2008; Cassat et al., 2003; Kim et al., 2006; Chowdhury, 2005]. Mellor and Tuner [1991] developed an accurate analytical thermal model. However, it is difficult to calculate all the parameters of the model due to the complex geometry, taking into account both axial and radial heat transfer and complicated heat convection in a totally enclosed fan cooled (TEFC) electrical machine.

A simplified thermal model for surface mounted PM synchronous motor (SPMSM) is developed in this paper. Due to the high conductivity of the rare-earth magnet, neodymium-iron-boron (NdFeB), and slot/tooth harmonics, there is eddy current loss generated inside the magnets. This loss may not attribute very much to the efficiency of the motor, but the temperature-rise inside the magnets caused by this loss can lead to the unpredictable deterioration of the magnets. In addition, the output voltage of pulse-width-modulated (PWM) inverter contains abundant high frequency harmonics, which induce additional losses in the motor [Ruifang et al., 2008; Ding and Mi, 2009]. Therefore, in this paper, the thermal circuit encompasses the eddy current loss in the magnets and PWM losses that still has not been considered in technical papers published.

In addition to the aforementioned losses, the other losses within the motor are considered. This is represented through a thermal circuit that incorporates conduction and convection behavior and the thermal resistances of the motor. Radiation is neglected due to the minor effect it has on such a system and for purposes of providing an accurate, but simple model. Moreover, the model developed permits the temperature profiles of SPMSM to be predicted analytically. The thermal circuits are then solved in MATLAB through a system of linear equations. FEA is also adopted in this paper to depict the temperature rise of SPMSM and to gain confidence of the analytical method.

2. LUMPED-PARAMETER THERMAL MODEL

The thermal resistances in the lumped-parameter representation circumscribe the paths for heat transfer and are analogous to the resistances in the electrical circuit. The model thereby establishes the equivalent parameters between the thermal and electrical domain as shown in Table 1.

Table 1 Analogy of thermal and electrical

Electrical circuit	Thermal circuit
Electric voltage u [V]	Temperature T [°*C*]
Current I [A]	Heat loss Q [W]
Electrical resistance R [Ohm]	Thermal resistance R [°*C*/W]
Electrical conductivity σ [S/m]	Thermal conductivity k [W/m°*C*]

The analogy allows the development of a lumped-parameter thermal model for SPMSM as shown in Figure 1. The thermal capacitances have been neglected since only steady state operation of the machine is considered. T_{in}, T_{stator}, T_{magnet}, T_{rotor}, T_w, T_{shaft} describe the temperatures of inner surface of insulation between stator and casing, inner surface of the stator core, outer surface of magnet, outer surface of rotor, the part of winding within the stator core and the part of shaft under rotor core respectively. $T_{coolant}$ and T_{case} are assigned as boundary conditions. Furthermore, the use of the individual thermal resistances as illustrated in Table 2 facilitates the development of the distinct analytical expressions (1)-(11).

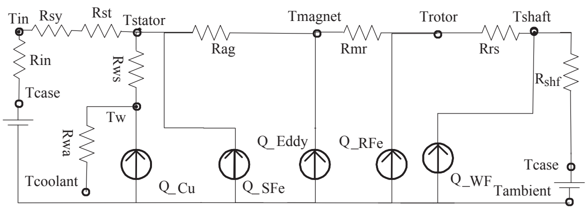

Fig. 1 Equivalent circuit mode

Table 2 Thermal resistances

Name	Depiction
R_{ag}	Convection thermal resistance of air gap
R_{mr}	Radial conduction thermal resistance of the pole
R_{rs}	Radial conduction thermal resistance of rotor core
R_{shf}	Thermal resistance of the shaft
R_{sy}	Radial conduction thermal resistance of stator yoke
R_{st}	Radial conduction thermal resistance of stator teeth
R_{ws}	Conduction thermal resistance between windings and stator
R_{in}	Contact thermal resistance between stator and housing

2.1 The thermal resistance of air gap - R_{ag}

Within the air gap the heat flow is greater than the adjoining air as almost 99 % heat emitted from the rotor surface would be transferred directly across it to stator.

Taylor [1935] developed the dimensionless convection correlation from testing on two concentric cylinders rotating relative to each other to consider the heat transfer across the air gap and further modified by Gazley [1958]. The thermal resistance can be defined in terms of the air gap length l_g, a dimensionless Nusselt number N_{nu}, thermal conductivity of motionless air K_{air} and average area of the air gap cylindrical surface A_{ag}.

$$R_{ag} = \frac{l_g}{N_{nu} K_{air} A_{ag}}$$

$$\begin{array}{ll} N_{nu} = 2 & N_{Ta} \le 41 \\ N_{nu} = 0.212 N_{Ta}^{0.63} N_{\mathrm{Pr}}^{0.27} & 41 < N_{Ta} \le 100 \\ N_{nu} = 0.386 N_{Ta}^{0.5} N_{\mathrm{Pr}}^{0.27} & N_{Ta} \le 41 \end{array} \tag{1}$$

The value of the Nusselt N_{nu}, Taylor N_{Ta} and Prandtl N_{Pr} numbers for two rotating smooth cylinders are presented by Taylor. The flow in air gap is laminar when N_{Ta} < 41 whereas the flow through the vortex with enhanced heat transfer ranges 41 < N_{TA} < 100. If N_{Ta} > 100 there is a fully turbulent flow in the air gap. Later, Gazley [1958] modified the heat transfer with a 10 % increase due to the slot effects through experimental results.

The expression given in (1) is applicable to air cooled electrical motors. In order to analyze oil cooled motors, the thermal conductivity of the air gap assumed as a constant value, one equivalent air gap resistance can be calculated considering the air gap equal to a cylinder. Reference [Hsu et al., 2005] shows that the thermal conductivity of Toyota Prius traction motor is 10 W/m-°*C* based on the oil and air convective mixture. In this case, the simpler expression for deriving the air gap thermal resistance is given as follows:

$$R_{ag2} = \frac{\ln(r_{is} / r_{magnet})}{2\pi k_{ag} L_g} \tag{2}$$

where

r_{magnet} the outer magnet radius;

r_{is} the inner stator radius;

k_{ag} thermal conductivity of the air gap.

2.2 The radial conduction thermal resistance of rotor core - R_{rs}

Figure 2 shows the rotor core as a cylinder made of laminations. The radial heat transfer is more pronounced than the axial heat transfer in the laminations therefore the heat transfer coefficient is calculated for the radial direction.

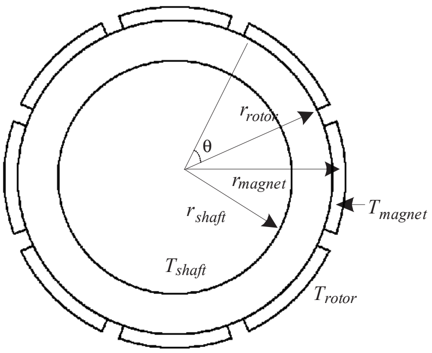

Fig. 2 Radial dimensions of the rotor dimensions of the rotor

$$R_{rs} = \frac{\ln(r_{rotor} / r_{shaft})}{2\pi k_{rotor} L_s} \tag{3}$$

where

r_{shaft} the shaft radius;

k_{rotor} thermal conductivity of rotor core;

L_s axial length of rotor core.

2.3 The radial conduction thermal resistance of the poles - R_{mr}

The surface-mounted magnets distributed on the rotor core are assumed as an equivalent cylinder with $n\theta$ radian.

$$R_{mr} = \frac{\ln(r_{magnet} / r_{rotor})}{n\theta k_m L_s} \tag{4}$$

where

r_{magnet} the outer rotor radius;

r_{rotor} the rotor core radius;

n number of poles;

θ radian of one pole;

k_m thermal conductivity of magnet;

L_s axial length of the poles.

2.4 The thermal resistance of the shaft - R_{shf}

The shaft represented as a cylindrical rod with axial heat conduction is separated to three parts [Mellor et al., 1991]: one that lies under the rotor core; a second that lies under the bearing; and a third that acts as a thermal connection between the mean temperatures of the above two. As the bearings provide good thermal contact, it is sufficient to consider thermal contact that exists between the shaft and the thermal casing. And the convection between shaft and adjoining air is neglected as the heat transfer from the air to the shaft is negligible.

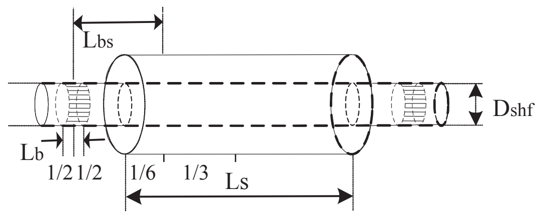

Fig. 3 Axial dimensions of the shaft

$$R_{shf} = (R_a + R_b) / 2 \tag{5}$$

where

$$R_a = \frac{1}{2\pi k_{shf} L_s} + \frac{L_{bs}}{2\pi k_{shf} (D_{shf}/2)^2}$$

$$R_b = \frac{1}{4\pi k_{shf} L_b} + \frac{L_{bs}}{2\pi k_{shf} (D_{shf}/2)^2}$$

k_{shf} thermal conductivity of shaft;

L_b thickness of bearing;

D_{shf} radius of shaft;

L_{bs} distance of bearing centre to rotor mean.

2.5 The radial conduction thermal resistance of stator teeth - R_{st}

As both the rotor and stator core consist of layers of laminations, only the thermal conductivity in the radial direction is considered. In order to calculate the thermal resistance of the stator precisely, the stator is modeled as two parts, one is the stator yoke and another is the stator teeth. The equivalent cylinder with a reduction factor is used to model the stator teeth.

$$R_{st} = \frac{\ln(r_{ms} / r_{is})}{2\pi k_{iro} L_s p} \tag{6}$$

where

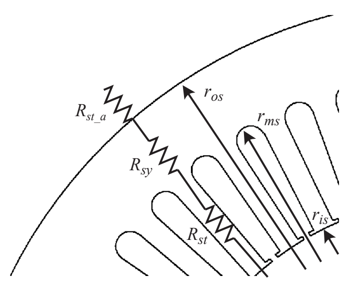

Fig. 4 Radial dimensions of the stator

r_{is} the inner stator radius;
r_{ms} the inner stator yoke radius;
k_{iro} thermal conductivity of stator.
p percentage of the teeth section respect to the total teeth plus all slots section.

2.6 The radial conduction thermal resistance of stator yoke - R_{sy}

$$R_{sy} = \frac{\ln(r_{os} / r_{ms})}{2\pi k_{iro} L_s} \quad (7)$$

where
r_{os} the outer stator yoke radius;

2.7 The conduction thermal resistance between windings and stator - R_{ws}

$$R_{ws} = \frac{S_{slot} - S_{cu}}{l_s k_{cu,ir} A_{slot}} \quad (8)$$

where
S_{slot} stator slot surface;
S_{cu} copper section in stator slot;
l_s stator slot perimeter;
$k_{cu,ir}$ equivalent conductivity coefficient of the air and insulation material in stator slot, evaluated by simulation;
A_{slot} $= l_s L_S$ interior slot surface.

2.8 Convective thermal resistance between winding external to stator and adjoining air - R_{wa}

The convection coefficient between the end winding of the stator and adjoining air is found [Mellor et al., 1991],

$$h_{wa} = 15.5(0.29v + 1) \quad (9)$$

where,
v and the speed of inner air needs no more than 7.5 m/s;
ω the rotor angular velocity;
η fan efficiency.

The value of 50 % was assumed for the fan efficiency usually due to unavailable information on the radial air velocity. Sometimes, there is oil and air mixture adjoining to the winding, a equivalent increase of fan efficiency is used.

The total surface of the winding external to stator can be calculated as

$$S_{wa} = (L_c - L_s)2\pi r_{is} \quad (10)$$

where L_c external casing length.

Therefore, from (9) and (10), the thermal resistance between winding external to stator and adjoining air can be calculated,

$$R_{wa} = \frac{1}{S_{wa} h_{wa}} \quad (11)$$

3. HEAT SOURCES

The thermal model is applied to a medium size SPMSM. Figure 5 shows the cross sectional view of a 3-phase 8-pole motor. Table 3 shows the basic parameters of the motor.

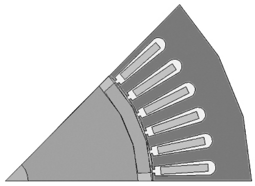

Fig. 5 The cross sectional of SPMSM

Table 3 Parameters of the motor

Parameters	Value
Rated speed	3600 rpm
Slot fill factor, rs	73.6 %
Pole Count, 2pr	8
Total Number of Slots, Qs	48
Magnet outer radius, Rm	73.69 mm
Magnet inner radius, Rr	80.2 mm
Stator bore radius, Rs	81 mm
Pole embrace, pe	0.86
Length, L	84 mm
Slot opening, b0	1.93 mm
Magnet electrical conductivity,	6.9×10^5 S/m
Slots per pole per phase number, q	2
Series turns per phase, N	32
Conductors per slot	16

PWM inverters are used in greater frequency to operate electrical machines in hybrid vehicle, with the advancements in power electronics. A limitation though with such technologies is the abundant high frequency harmonics in the output voltage of PWM inverter which induce additional losses. The eddy current loss due to the PWM supply is 2.53 times the loss under pure sine wave supply [Liu et al., 2008]. Therefore, a proportional rise in the temperatures of electrical machines can be observed. It's critical to predict the losses caused by PWM supply. The losses with the motor are modeled as heat sources (Q) in the equivalent circuit. This circuit can be incorporated into the separate frameworks of a sine waveform supply and PWM waveform supply.

In order to compare the increment of losses under PWM supply, the fundamental frequency and amplitude are the same with the pure sinusoidal waveform. The frequency modulation ratio R ($R = f_c / f_1$, f_c is switching frequency of the triangle waveform and is frequency of the fundamental sinusoidal modulation waveform) and the amplitude modulation ratio M ($M = V_1 / V_c$, V_1 is the amplitude of the sinusoidal waveform and is the amplitude of triangle waveform) are set as 15 and 0.9 respectively, which are observed in Figure 6.

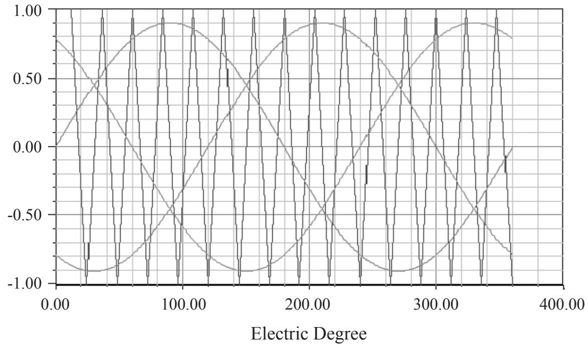

Fig. 6 The triangle and fundamental sinusoidal modulation waveform

Table 4 shows the losses in the motor from PWM waveform are twofold in magnitude in relation to the losses under sinusoidal, the exception being the copper loss, friction and windage losses. These results are consistent with the previous work [Liu et al., 2008; Ding and Mi, 2009].

Table 4 Losses under sine and PWM waveform

	Sinusoidal	PWM
Input power	53.586 kW	53.706 kW
Output power	51.644 kW	50.136 kW
Efficiency	96.4 %	93.4 %
Stator iron loss	1.091 kW	2.723 kW
Stator copper loss	0.245 kW	0.253 kW
Rotor iron loss	0.188 kW	0.345 kW
Friction and windage loss	0.316 kW	0.316 kW
Eddy current loss in the magnets	0.102 kW	0.249 kW

4. COMPARISONS BETWEEN SIMULATION AND ANALYTICAL METHOD

Assigning the losses and casing temperature (90 °C) to the thermal circuit, the temperature of individual components in the motor can be obtained after the calculation. The simulation using Ansoft ePhysics is also developed to confirm the analytical method.

Consider the equivalent circuit model in Figure 1.

At node *Tin*

$$\frac{Tstator - Tin}{Rsy + Rst} - \frac{Tin - Tcase}{Rin} = 0 \tag{12}$$

At node

$$\frac{Tstator - Tin}{Rsy + Rst} - \frac{Tw - Tstator}{Rws} \frac{Tmagnet - Tstator}{Rag} = Q\_SFe \tag{13}$$

At node

$$\frac{Tw - Tstator}{Rws} - \frac{Tw - Tcoolant}{Rwa} = Q\_Cu \tag{14}$$

At node

$$\frac{Tmagnet - Tstator}{Rag} - \frac{Trotor - Tmagnet}{Rmr} = Q\_Eddy \tag{15}$$

At node

$$\frac{Trotor - Tshaft}{Rrs} + \frac{Trotor - Tmagnet}{Rmr} = Q\_RFe + Q\_WF \tag{16}$$

At node

$$\frac{Trotor - Tshaft}{Rrs} - \frac{Tshaft - Tcase}{Rshf} = 0 \tag{17}$$

A matrix (18) obtained from the equations (12)-(17) can be used to calculate the node temperatures. From section 2, $k_{cu,ir}$ is equivalent conductivity coefficient of the air and insulation material in stator slot and could not be computed directly. A programme for solving the matrix is developed in Matlab, the value of $k_{cu,ir}$ is changed until the computed temperatures are comparable with the simulation ones. Table 5 show the results when $k_{cu,ir} = 0.408$.

Figure 7 depicts the temperature profile of the magnet using Ansoft ePhysics. The magnet exhibits a discernable radial temperature gradient with the hotter portion evident in the base of the magnet. The upper surface of the magnet is cooler due the convection with the air and oil mixture in the air gap. In addition, heat is transferred from magnet to the stator through the air gap further affecting the temperature distribution.

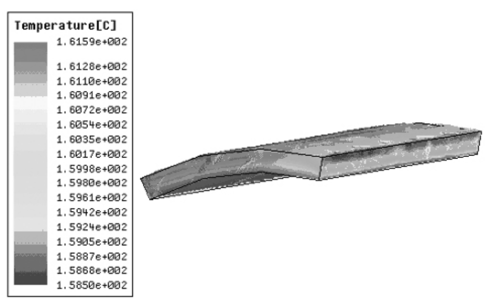

Fig. 7 Temperature profiles in magnet

Table 5 shows the comparison of temperature distribution within the motor from the analytical method and simulation. And the two results agree well. The node Tw indicates a portion of the winding temperature based on a selected geometry in equivalent circuit. However, the simulation shows the connection parts are hotter based on the value of convection resistance (R_{wa}) is smaller than the conduction resistance (R_{ws}).

Table 5 Temperature distribution within the motor fed by sine waveform

Name	Analytical method (°*C*)	Simulation (°*C*)
Insulation	90-113.23	90-119.45
Stator	113.23-152.35	120.21-156.73
Winding	155.29	162.63-180.39
Magnets	154.88-155.47	158.68-161.13
Rotor	155.47-169.76	156.34-162.90
shaft	90-169..76	90-163.58

Table 6 Temperature distribution under sinusoidal and PWM waveform

Name	Sine (°*C*)	PWM (°*C*)
Insulation	90-113.23	90-159.14
Stator	113.23-152.35	159.14-198.25
Winding	155.29	202.47
Magnets	154.88-155.47	200.92-201.54
Rotor	155.47-169.76	201.54-213.83
shaft	90-169.76	90-213.83

The simulation results verify the analytical method under sine supply. Therefore assigning the losses under PWM waveform to the thermal circuit, the temperature profiles under PWM supply can be obtained. The temperature rises dramatically due to additional losses under PWM.

The hottest portion of magnets ascend to 201.54 °C, which will induce the irreversible demagnetization. These results provide the crucial information for the motor design. Minimization of the losses within the motor [Mi et al., 2005; Zhang et al., 2007; Park et al., 2008; Yamazaki and Ishigami, 2008] and improvement of the coolant system can be used to restrain the temperature rise.

5. CONCLUSION

The thermal model of SPMSM is represented as network resistances, temperature nodes and heat flux sources. A simplified model has been developed to provide an estimation of the temperature rise in individual components of the SPMSM. The model considers the losses (heat sources including eddy current loss) in the thermal circuit along with the sinusoidal and PWM waveforms respectively. The analytical model is substantiated by means of an FEA simulation providing a reliable method to predict the temperature rise. It is shown that temperature rise can exceed the limit which can cause potential demagnetizing of the magnets. This temperature rise due to additional losses generated by PWM supply needs to be considered in the very beginning stage of the motor design.

REFERENCES

Boglietti, A., A. Cavagnino, M. Lazzari, and M. Pastorelli, A simplified thermal model for variable speed self cooled industrial induction motor, *Proceedings of IEEE Industry Applications Conference 37th IAS Annual Meeting*, Vol. 2, 723-730, 2002.

Cassat, A., C. Espanet, and N. Wavre, BLDC motor stator and rotor iron losses and thermal behavior based on lumped schemes and 3-D FEM analysis, *Proceedings of IEEE Transactions on Industry Applications*, Vol. 39, No. 5, 1314-1322, 2003.

Chowdhury, S. K., A distributed parameter thermal model for induction motors, *Proceeding of Power Electronics and Drives Systems 2005*, Vol. 1, 739-744, 2005.

Ding, X. F., and C. Mi, Modeling of eddy current loss in the magnets of permanent magnet machines for hybrid and electric vehicle traction applications, *Proceedings of IEEE Vehicle Power and Propulsion Conference 2009*, 419-424, 2009.

Funieru, B., and A. Binder, Thermal design of a permanent magnet motor used for gearless railway traction, *Proceedings of 34th Annual Conference of the IEEE Industrial Electronics Society*, 2061-2066, 2008.

Gazley, C., Heat transfer characteristics of rotational and axial flow between concentric cylinder, *Transaction of the ASME*, 79-89, 1958.

Guo, Y. G., J. G. Zhu, and W. Wu, Thermal analysis of soft magnetic composite motors using a hybrid

$$\begin{bmatrix} -1/(Rsy+Rst)-1/Rin & 1/(Rsy+Rst) & 0 & 0 & 0 & 0 \\ -1/(Rsy+Rst) & 1/Rag+1/(Rsy+Rst)+1/Rws & -1/Rws & -1/Rag & 0 & 0 \\ 0 & -1/Rws & 1/Rws & 0 & 0 & 0 \\ 0 & -1/Rag & 0 & 1/Rmr+1/Rag & -1/Rmr & 0 \\ 0 & 0 & 0 & -1/Rmr & -1/Rrs+1/Rmr & -1/Rrs \\ 0 & 0 & 0 & 0 & 1/Rrs & -1/Rrs-1/Rshf \end{bmatrix} * \begin{bmatrix} Tin \\ Tstator \\ Tw \\ Tmagnet \\ Trotor \\ Tshaft \end{bmatrix} = \begin{bmatrix} -90/Rin \\ Q\_SFe \\ Q\_cu+110/Rwa \\ Q\_Eddy \\ Q\_RFe \\ Q\_WF+90/Rshf \end{bmatrix} \quad (18)$$

model with distributed heat sources, *IEEE Transactions on Magnetics*, Vol. 41, No. 6, 2124-2128, 2005.

Hsu, J. S., S. C. Nelson, P. A. Jallouk, C. W. Ayers, R. H. Wiles, S. L. Campbell, C. L. Coomer, K. T. Lowe, and T. A. Burress, *Report on Toyota Prius Motor Thermal Management*, 2005.

Ishak, D., Z. Q. Zhu, and D. Howe, Eddy-current loss in the rotor magnets of permanent-magnet brushless machines having a fractional number of slots per pole, *IEEE Transactions on Magnetics*, Vol. 41, No. 9, 3728-3726, 2005.

Kim, W. G., J. I. Lee, K. W. Kim, Y. S. Kim, and C. D. Lee, The temperature rise characteristic analysis technique of the traction motor for EV application, *Proceedings of First International Forum on Strategic Technology*, 443-446, 2006.

Liu, R. F., C. C. Mi, and D. W. Gao, Modeling of eddy-current loss of electrical machines and transformers operated by pulse width-modulated inverters, *IEEE Transactions on Magnetics*, Vol. 44, No. 8, 2021-2028, 2008.

Mellor, P. H., D. Roberts, and D. R. Turner, Lumped parameter thermal model for electrical machines of TEFC design, *Electric Power Applications, IEE Proceedings B*, Vol. 138, No.5, 205-218, 1991.

Mi, C. C., G. R. Slemon, and R. Bonert, Minimization of iron losses of permanent magnet synchronous machines, *IEEE Transactions on Energy Conversion*, Vol. 20, No. 1, 121-127, 2005.

Park, J. D., C. Kalev, and H. F. Hofmann, Analysis and reduction of time harmonic rotor loss in solid-rotor synchronous reluctance drive, *IEEE Transactions on Power Electronics*, Vol. 23, No. 2, 985-992, 2008.

Sai, C. T., T. A. Keim, and D. J. Perreault, Thermal modeling of Lundell alternators, IEEE Transactions on Energy Conversion, Vol. 20, No. 1, 25-36, 2005.

Sooriyakumar, G., R. Perryman, and S. J. Dodds, Analytical thermal modelling for permanent magnet synchronous motors, *Proceedings of 42nd International Universities Power Engineering Conference*, 192-196, 2007.

Staton, D. A., and A. Cavagnino, Convection heat transfer and flow calculations suitable for electric machines thermal models, *IEEE Transactions on Industrial Electronics*, Vol. 55, No. 10, 3509-3516, 2008.

Staton, D., A. Boglietti, and A. Cavagnino, Solving the more difficult aspects of electric motor thermal analysis in small and medium size industrial induction motors, *IEEE Transactions on Energy Conversion*, Vol. 20, No. 3, 620-628, 2005.

Taylor, G. I., Distribution of velocity and temperature between concentric cylinders, *Proceedings of the Royal Society of London. Series A, Mathematical and Physical Sciences*, Vol. 151, Issue 874, 494-512, 1935.

Yamazaki, K., and H. Ishigami, Reduction of harmonic iron losses in interior permanent magnet motors by optimization of rotor structures, *Proceedings of Electrical Machines and Systems 2008*, 2870-2875, 2008.

Yoshida, K., Y. Hita, and K. Kesamaru, Eddy-current loss analysis in PM of surface-mounted-PM SM for electric vehicles, *IEEE Transactions on Magnetics*, Vol. 36, 1941-1944, 2000.

Zhang, G. W., F. X. Wang, and Y. S. Shen, Reduction of rotor loss and cogging torque of high speed PM machine by stator teeth notching, *Proceedings of Electrical Machines and Systems 2007*, 856-859, 2007.

(Received April 8, 2010; accepted April 15, 2010)